

# A PRECONDITIONER FOR A PRIMAL-DUAL NEWTON CONJUGATE GRADIENTS METHOD FOR COMPRESSED SENSING PROBLEMS

December 30, 2014

IOANNIS DASSIOS\*, KIMON FOUNTOLAKIS†, AND JACEK GONDZIO‡

**Abstract.** In this paper we are concerned with the solution of Compressed Sensing (CS) problems where the signals to be recovered are sparse in coherent and redundant dictionaries. We extend the primal-dual Newton Conjugate Gradients (pdNCG) method in [9] for CS problems. We provide an inexpensive and provably effective preconditioning technique for linear systems using pdNCG. Numerical results are presented on CS problems which demonstrate the performance of pdNCG with the proposed preconditioner compared to state-of-the-art existing solvers.

**Key words.** compressed sensing,  $\ell_1$ -analysis, total-variation, second-order methods, Newton conjugate gradients

**1. Introduction.** CS is concerned with recovering a signal  $\tilde{x} \in \mathbb{R}^n$  by observing a linear combination of the signal

$$\tilde{b} = A\tilde{x},$$

where  $A \in \mathbb{R}^{m \times n}$  is an under-determined linear operator with  $m < n$  and  $\tilde{b} \in \mathbb{R}^m$  are the observed measurements. Although this system has infinitely many solutions, reconstruction of  $\tilde{x}$  is possible due to its assumed properties. In particular,  $\tilde{x}$  is assumed to have a sparse image through a redundant and coherent dictionary  $W \in E^{n \times l}$ , where  $E = \mathbb{R}$  or  $\mathbb{C}$  and  $n \leq l$ . More precisely,  $W^*\tilde{x}$ , is sparse, i.e. it has only few non-zero components, where the star superscript denotes the conjugate transpose. If  $W^*\tilde{x}$  is sparse, under certain conditions on matrices  $A$  and  $W$  (discussed in Subsection 1.2) the optimal solution of the linear  $\ell_1$ -analysis problem

$$\text{minimize } \|W^*x\|_1, \quad \text{subject to: } Ax = \tilde{b}$$

is  $\tilde{x}$ , where  $\|\cdot\|_1$  is the  $\ell_1$ -norm.

Frequently measurements  $\tilde{b}$  might be contaminated with noise, i.e. one measures  $b = \tilde{b} + e$  instead, where  $e$  is a vector of noise, usually modelled as Gaussian with zero-mean and bounded Euclidean norm. In addition, in realistic applications,  $W^*\tilde{x}$  might not be exactly sparse, but its mass might be concentrated only on few of its components, while the rest are rapidly decaying. In this case, (again under certain conditions on matrices  $A$  and  $W$ ) the optimal solution of the following  $\ell_1$ -analysis problem

$$(1.1) \quad \text{minimize } f_c(x) := c\|W^*x\|_1 + \frac{1}{2}\|Ax - b\|_2^2,$$

\*I. Dassios is with the School of Mathematics and Maxwell Institute, The University of Edinburgh, Peter Guthrie Tait Road, Edinburgh EH9 3FD, United Kingdom e-mail: idassios@ed.ac.uk. I. Dassios is supported by EPSRC Grant EP/I017127/1

†K. Fountoulakis is with the School of Mathematics and Maxwell Institute, The University of Edinburgh, Peter Guthrie Tait Road, Edinburgh EH9 3FD, United Kingdom e-mail: K.Fountoulakis@sms.ed.ac.uk.

‡J. Gondzio is with the School of Mathematics and Maxwell Institute, The University of Edinburgh, Peter Guthrie Tait Road, Edinburgh EH9 3FD, United Kingdom e-mail: J.Gondzio@ed.ac.uk.

is proved to be a good approximation to  $\tilde{x}$ . In (1.1),  $c$  is an a-priori chosen positive scalar and  $\|\cdot\|_2$  is the Euclidean norm.

**1.1. Brief description of CS applications.** An example of  $W$  being redundant and coherent with orthonormal rows is the curvelet frame where an image is assumed to have an approximately sparse representation [6]. Moreover, for radar and sonar systems it is frequent that Gabor frames are used in order to reconstruct pulse trains from CS measurements [19]. For more applications a small survey is given in [7]. Isotropic Total-Variation (iTV) is another application of CS, which exploits the fact that digital images frequently have slowly varying pixels, except along edges. This property implies that digital images with respect to the discrete nabla operator, i.e. local differences of pixels, are approximately sparse. For iTV applications, matrix  $W \in \mathbb{C}^{n \times n}$  is square, complex and rank-deficient with  $\text{rank}(W) = n - 1$ . An alternative to iTV is  $\ell_1$ -analysis, where matrix  $W$  is a Haar wavelet transform. However, a more pleasant to the eye reconstruction is obtained by solving the iTV problem compared to the  $\ell_1$ -analysis problem, see [21].

**1.2. Conditions and properties of CS matrices.** There has been an extensive amount of literature studying conditions and properties of matrices  $A$  and  $W$  which guarantee recoverability of a good approximation of  $\tilde{x}$  by solving problem (1.1). For a thorough analysis we refer the reader to [7, 21]. The previously cited papers use a version of the well-known *Restricted Isometry Property* (RIP) [7], which is repeated below.

DEFINITION 1.1. *The restricted isometry constant of a matrix  $A \in \mathbb{R}^{m \times n}$  adapted to  $W \in E^{n \times l}$  is defined as the smallest  $\delta_q$  such that*

$$(1 - \delta_q)\|Wz\|_2^2 \leq \|AWz\|_2^2 \leq (1 + \delta_q)\|Wz\|_2^2$$

for all at most  $q$ -sparse  $z \in E^l$ , where  $E = \mathbb{R}$  or  $\mathbb{C}$ .

For the rest of the paper we will refer to Definition 1.1 as W-RIP. It is proved in Theorem 1.4 in [7] that if  $W \in E^{n \times l}$  has orthonormal rows with  $n \leq l$  and if  $A, W$  satisfy the W-RIP with  $\delta_{2q} \leq 8.0e-2$ , then the solution  $x_c$  obtained by solving problem (1.1) satisfies

$$(1.2) \quad \|x_c - \tilde{x}\|_2 = C_0\|e\|_2 + C_1 \frac{\|W^*x_c - (W^*\tilde{x})_q\|_1}{\sqrt{q}},$$

where  $(W^*\tilde{x})_q$  is the best  $q$ -sparse approximation of  $W^*\tilde{x}$ ,  $C_0$  and  $C_1$  are small constants and only depend on  $\delta_{2q}$ . It is clear that  $W^*\tilde{x}$  must have  $l - q$  rapidly decaying components, in order for  $\|x_c - \tilde{x}\|_2$  to be small and the reconstruction to be successful. iTV is a special case of  $\ell_1$ -analysis where matrix  $W$  does not have orthonormal rows, hence, result (1.2) does not hold. For iTV there are no conditions on  $\delta_{2q}$  such that a good reconstruction is assured. However, there exist results which directly impose restrictions on the number of measurements  $m$ , see Theorems 2, 5 and 6 in [21]. Briefly, in these theorems it is mentioned that if  $m \geq q \log(n)$  linear measurements are acquired for which matrices  $A$  and  $W$  satisfy the W-RIP for some  $\delta_q < 1$ , then, similar reconstruction guarantees as in (1.2) are obtained for iTV. Based on the previously mentioned results regarding reconstruction guarantees it is natural to assume that for iTV a similar condition applies, i.e.  $\delta_{2q} < 1/2$ . Hence, we make the following assumption.

ASSUMPTION 1.2. *The number of nonzero components of  $W^*x_c$ , denoted by  $q$ , and the dimensions  $l, m, n$  are such that matrices  $A$  and  $W$  satisfy W-RIP for some*

$\delta_{2q} < 1/2$ . This assumption will be used in the spectral analysis of our preconditioner in Section 5.

Another property of matrix  $A$  is the near orthogonality of its rows. Indeed many applications in CS use matrices  $A$  that satisfy

$$(1.3) \quad \|AA^\top - I_m\|_2 \leq \delta,$$

with a small constant  $\delta \geq 0$ . Finally, through the paper we will make use of the following assumption

$$(1.4) \quad \text{Ker}(W^*) \cap \text{Ker}(A) = \{0\},$$

This is commonly used assumption in the literature, see for example [24].

**1.3. Contribution.** In [9], Chan, Golub and Mulet, proposed a primal-dual Newton Conjugate Gradients method for image denoising and deblurring problems. In this paper we modify their method and adapt it for CS problems with coherent and redundant dictionaries. There are two major contributions.

First, we propose an inexpensive preconditioner for fast solution of systems using pdNCG when applied to CS problems with coherent and redundant dictionaries. We analyze the limiting behaviour of our preconditioner and prove that the eigenvalues of the preconditioned matrices are clustered around one. This is an essential property that guarantees that only a few iterations of CG will be needed to approximately solve the linear systems. Moreover, we provide computational evidence that the preconditioner works well not only close to the solution (as predicted by its spectral analysis) but also in earlier iterations of pdNCG.

Second, we demonstrate that despite being a second-order method, pdNCG can be more efficient than specialized first-order methods for CS problems of our interest, even on large-scale instances. This performance is observed in several numerical experiments presented in this paper. We believe that the reason for this is that pdNCG, as a second-order method, captures the curvature of the problems, which results in sufficient decrease in the number of iterations compared to first-order methods. This advantage comes with the computational cost of having to solve a linear system at every iteration. However, inexact solution of the linear systems using CG combined with the proposed efficient preconditioner crucially reduces the computational costs per iteration.

**1.4. Format of the paper and notation.** The paper is organized as follows. In Section 2, problem (1.1) is replaced by a smooth approximation; the  $\ell_1$ -norm is approximated by the pseudo-Huber function. Derivation of pseudo-Huber function is discussed and its derivatives are calculated. In Section 3, a primal-dual reformulation of the approximation to problem (1.1) and its optimality conditions are obtained. In Section 4, pdNCG is presented. For convergence analysis of pdNCG method the reader is referred to [9, 13]. In Section 5, a preconditioning technique is described for controlling the spectrum of matrices in systems which arise. In Section 6, a continuation framework for pdNCG is described. In Section 7, numerical experiments are discussed that present the efficiency of pdNCG. Finally, in Section 8, conclusions are made.

Throughout the paper,  $\|\cdot\|_1$  is the  $\ell_1$ -norm,  $\|\cdot\|_2$  is the Euclidean norm,  $\|\cdot\|_\infty$  the infinity norm and  $|\cdot|$  is the absolute value. The functions  $Re(\cdot)$  and  $Im(\cdot)$  take a complex input and return its real and imaginary part, respectively. For simplification

of notation, occasionally we will use  $Re(\cdot)$  and  $Im(\cdot)$  without the parenthesis. Furthermore,  $diag(\cdot)$  denotes the function which takes as input a vector and outputs a diagonal square matrix with the vector in the main diagonal. Finally, the super index  $c$  denotes the complementarity set, i.e.  $\mathcal{B}^c$  is the complement set of  $\mathcal{B}$ .

**2. Regularization by pseudo-Huber.** In pdNCG [9] the non-differentiability of the  $\ell_1$ -norm is treated by applying smoothing. In particular, the  $\ell_1$ -norm is replaced with the pseudo-Huber function [16]

$$(2.1) \quad \psi_\mu(W^*x) := \sum_{i=1}^l ((\mu^2 + |W_i^*x|^2)^{\frac{1}{2}} - \mu),$$

where  $W_i$  is the  $i^{th}$  row of matrix  $W \in E^{n \times l}$  and  $\mu$  controls the quality of approximation, i.e. for  $\mu \rightarrow 0$ ,  $\psi_\mu(x)$  tends to the  $\ell_1$ -norm. The original problem (1.1) is approximated by

$$(2.2) \quad \text{minimize } f_c^\mu(x) := c\psi_\mu(W^*x) + \frac{1}{2}\|Ax - b\|_2^2.$$

**2.1. Derivation of pseudo-Huber function.** The pseudo-Huber function (2.1) can be derived in a few simple steps. First, we re-write function  $\|W^*x\|_1$  in its dual form

$$(2.3) \quad \|W^*x\|_1 = \sup_{g \in \mathbb{C}^l, \|g\|_\infty \leq 1} Re(\bar{g}^* W^*x),$$

where  $g$  are dual variables. The pseudo-Huber function is obtained by regularizing the previous dual form

$$(2.4) \quad \psi_\mu(W^*x) = \sup_{g \in \mathbb{C}^l, \|g\|_\infty \leq 1} Re(\bar{g}^* W^*x) + \sum_{i=1}^l \left( \mu(1 - |g_i|^2)^{\frac{1}{2}} - \mu \right),$$

where  $g_i$  is the  $i^{th}$  component of vector  $g$ .

An approach which consists of smoothing a non-smooth function through its dual form is known as Moreau's proximal smoothing technique [20]. Another way to smooth function  $\|W^*x\|_1$  is to regularize its dual form with a strongly convex quadratic function  $\mu/2\|g\|_2^2$ . Such an approach provides a smooth approximation of  $\|W^*x\|_1$  which is known as Huber function and it has been used in [4]. Generalizations of the Moreau proximal smoothing technique can be found in [22] and [3].

**2.2. Derivatives of pseudo-Huber function.** The gradient of pseudo-Huber function  $\psi_\mu(W^*x)$  in (2.1) is given by

$$\nabla \psi_\mu(W^*x) = Re(WDW^*)x,$$

where  $D := diag(D_1, D_2, \dots, D_l)$  with

$$(2.5) \quad D_i := (\mu^2 + |y_i|^2)^{-\frac{1}{2}} \quad \forall i = 1, 2, \dots, l,$$

and  $y = [y_1, y_2, \dots, y_l]^T := W^*x$ . The gradient of function  $f_c^\mu(x)$  in (2.2) is

$$\nabla f_c^\mu(x) = c\nabla \psi_\mu(W^*x) + A^T(Ax - b).$$

The Hessian matrix of  $\psi_\mu(x)$  is

$$(2.6) \quad \nabla^2 \psi_\mu(W^*x) := \frac{1}{4}(W\hat{Y}W^* + \bar{W}\hat{Y}\bar{W}^* + W\tilde{Y}\bar{W}^* + \bar{W}\tilde{Y}W^*),$$

where the bar symbol denotes the complex conjugate,  $\hat{Y} := \text{diag} [\hat{Y}_1, \hat{Y}_2, \dots, \hat{Y}_l]$ ,  $\tilde{Y} := \text{diag} [\tilde{Y}_1, \tilde{Y}_2, \dots, \tilde{Y}_l]$  and

$$(2.7) \quad \hat{Y}_i := \mu^2 D_i^3 + D_i, \quad \tilde{Y}_i := -y_i^2 D_i^3, \quad i = 1, 2, \dots, l,$$

Moreover, the Hessian matrix of  $f_c^\mu(x)$  is

$$(2.8) \quad \nabla^2 f_c^\mu(x) = c\nabla^2 \psi_\mu(W^*x) + A^\top A.$$

**3. Primal-dual formulation and optimality conditions.** In [8] the authors solved iTV problems for square and full-rank matrices  $A$  which were inexpensively diagonalizable, i.e. image deblurring or denoising. More precisely, in the previous cited paper the authors tackled iTV problems using a Newton-CG method to solve problem (2.2). They observed that close to the points of non-smoothness of the  $\ell_1$ -norm, the smooth pseudo-Huber function (2.1) exhibited an ill-conditioning behaviour. This results in two major drawbacks of the application of Newton-CG. First, the linear algebra is challenging. Second, the region of convergence of Newton-CG is substantially shrunk. To deal with these problems they proposed to incorporate Newton-CG inside a continuation procedure on the parameters  $c$  and  $\mu$ . Although they showed that continuation did improve the global convergence properties of Newton-CG it was later discussed in [9] (for the same iTV problems) that continuation was difficult to control (especially for small  $\mu$ ) and Newton-CG was not always convergent in reasonable CPU time.

In [9], Chan, Golub and Mulet provided numerical evidence that the behaviour of a Newton-CG method can be made significantly more robust even for small values of  $\mu$ . This is achieved by simply solving a primal-dual reformulation of (2.2), which is given below

$$(3.1) \quad \text{minimize} \quad \sup_{g \in \mathbb{C}^l, \|g\|_\infty \leq 1} c \text{Re}(\bar{g}^* W^*)x + c \sum_{i=1}^l \left( \mu(1 - |g_i|^2)^{1/2} - \mu \right) + \frac{1}{2} \|Ax - b\|_2^2.$$

The reason that Newton-CG method is more robust when applied on problem (3.1) than on problem (2.2) is hidden in the linearization of the optimality conditions of the two problems.

**3.1. Optimality conditions.** The optimality conditions of problem (2.2) are

$$(3.2) \quad \nabla \psi_\mu(W^*x) + A^\top(Ax - b) = c \text{Re}(WDW^*)x + A^\top(Ax - b) = 0.$$

The first-order optimality conditions of the primal-dual problem (3.1) are

$$(3.3) \quad \begin{aligned} c \text{Re}(W\bar{g}) + A^\top(Ax - b) &= 0, \\ D^{-1}\bar{g} &= W^*x. \end{aligned}$$

Notice for conditions (3.3) that the constraint  $\|g\|_\infty \leq 1$  in (3.1) is redundant since any  $x$  and  $g$  that satisfy (3.3) also satisfy this constraint. Hence, the constraint has

been dropped. Conditions (3.3) are obtained from (3.2) by simply setting  $\bar{g} = DW^*x$ . Hence, their only difference is the inversion of matrix  $D$ . However, this small difference affects crucially the performance of Newton-CG.

The reason behind this is that the linearization of the second equation in (3.3), i.e.  $D^{-1}\bar{g} = W^*x$ , is of much better quality than the linearization of  $\nabla\psi_\mu(W^*x)$  for  $\mu \approx 0$  and  $W^*x \approx 0$ . To see why this is true, observe that for small  $\mu$  and  $W^*x \approx 0$ , the gradient  $\nabla\psi_\mu(W^*x)$  becomes close to singular and its linearization is expected to be inaccurate. On the other hand,  $D^{-1}\bar{g} = W^*x$  as a function of  $W^*x$  is not singular for  $\mu \approx 0$  and  $W^*x \approx 0$ , hence, its linearization is expected to be more accurate. We refer the reader to Section 3 of [9] for empirical justification.

**4. Primal-dual Newton conjugate gradients method.** In this section we present details of pdNCG method [9].

**4.1. The method.** First, we convert optimality conditions (3.3) to the real case. This is done by splitting matrix  $W = \text{Re}W + \sqrt{-1}\text{Im}W$  and the dual variables  $g = g_{re} + \sqrt{-1}g_{im}$  into their real and imaginary parts. We do this in order to obtain optimality conditions which are differentiable in the classical sense of real analysis. This allows a straightforward application of pdNCG method [9]. The real optimality conditions of the primal-dual problem (3.1) are given below

$$(4.1) \quad \begin{aligned} c(\text{Re}Wg_{re} + \text{Im}Wg_{im}) + A^\top(Ax - b) &= 0, \\ D^{-1}g_{re} &= \text{Re}W^\top x, \quad D^{-1}g_{im} = \text{Im}W^\top x. \end{aligned}$$

At every iteration of pdNCG the primal-dual directions are calculated by approximate solving the following linearization of the equality constraints in (4.1)

$$(4.2) \quad \begin{aligned} B\Delta x &= -\nabla f_c^\mu(x) \\ \Delta g_{re} &= D(I - B_1)\text{Re}W^\top \Delta x + DB_2\text{Im}W^\top \Delta x - g_{re} + D\text{Re}W^\top x \\ \Delta g_{im} &= D(I - B_4)\text{Im}W^\top \Delta x + DB_3\text{Re}W^\top \Delta x - g_{im} + D\text{Im}W^\top x \end{aligned}$$

where

$$(4.3) \quad B := c\tilde{B} + A^\top A,$$

$$\begin{aligned} \tilde{B} &:= \text{Re}WD(I - B_1)\text{Re}W^\top + \text{Im}WD(I - B_4)\text{Im}W^\top + \text{Re}WDB_2\text{Im}W^\top \\ &\quad + \text{Im}WB_3D\text{Re}W^\top, \end{aligned}$$

and  $B_i, i = 1, 2, 3, 4$  are diagonal matrices with components

$$\begin{aligned} [B_1]_{ii} &:= D_i[g_{re}]_i \text{Re}W_i^\top x, & [B_2]_{ii} &:= D_i[g_{re}]_i \text{Im}W_i^\top x, \\ [B_3]_{ii} &:= D_i[g_{im}]_i \text{Re}W_i^\top x, & [B_4]_{ii} &:= D_i[g_{im}]_i \text{Im}W_i^\top x. \end{aligned}$$

**REMARK 4.1.** *Matrix  $B$  in (4.3) is positive definite (and invertible) if  $\|g_{re} + \sqrt{-1}g_{im}\|_\infty \leq 1$  and condition (1.4) are satisfied. The former condition will be maintained through all iterations of pdNCG.*

It is straightforward to show the claim in Remark 4.1 for the case of  $W$  being a real matrix. For the case of complex  $W$  we refer the reader to a similar claim which is made in [9], page 1970. Although matrix  $B$  is positive definite under the conditions stated in Remark 4.1, it is not symmetric, except in the case that  $W$  is

real where all imaginary parts are dropped. Therefore in the case of complex matrix  $W$ , preconditioned CG (PCG) cannot be employed to approximately solve (4.2). To avoid the problem of non-symmetric matrix  $B$  the authors in [9] suggested to ignore the non-symmetric part in matrix  $B$  and employ CG to solve (4.2). This idea is based on the following remark.

REMARK 4.2. *The symmetric part of  $B$  tends to the symmetric second-order derivative of  $f_c^\mu(x)$  as pdNCG converges (see Section 5 in [9]).*

Hence, system (4.2) is replaced with

$$(4.4) \quad \begin{aligned} \hat{B}\Delta x &= -\nabla f_c^\mu(x) \\ \Delta g_{re} &= D(I - B_1)ReW^\top \Delta x + DB_2ImW^\top \Delta x - g_{re} + DReW^\top x \\ \Delta g_{im} &= D(I - B_4)ImW^\top \Delta x + DB_3ReW^\top \Delta x - g_{im} + DImW^\top x \end{aligned}$$

where

$$(4.5) \quad \hat{B} := c \text{sym}(\tilde{B}) + A^\top A$$

and  $\text{sym}(\tilde{B}) := 1/2(\tilde{B} + \tilde{B}^\top)$  is the symmetric part of  $\tilde{B}$ . Moreover, PCG is terminated when

$$(4.6) \quad \|\hat{B}\Delta x + \nabla f_c^\mu(x)\|_2 \leq \eta \|\nabla f_c^\mu(x)\|_2,$$

is satisfied for  $\eta \in [0, 1)$ . Then the iterate  $g = g_{re} + \Delta g_{re} + \sqrt{-1}(g_{im} + \Delta g_{im})$  is orthogonally projected on the box  $\{x : \|x\|_\infty \leq 1\}$ . The projection operator for complex arguments is applied component-wise and it is defined as  $v := P_{\|\cdot\|_\infty \leq 1}(u) = \min(1/|u|, 1) \odot u$ , where  $\odot$  denotes the component-wise multiplication. In the last step, line-search is employed for the primal  $\Delta x$  direction in order to guarantee that the objective value  $f_c^\mu(x)$  is monotonically decreasing, see Section 5 of [9]. The pseudo-code of pdNCG is presented in Figure 4.1.

**5. Preconditioning.** Practical computational efficiency of pdNCG applied to system (4.4) depends on spectral properties of matrix  $\hat{B}$  in (4.5). Those can be improved by a suitable preconditioning. In this section we introduce a new preconditioner for  $\hat{B}$  and discuss the limiting behaviour of the spectrum of preconditioned  $\hat{B}$ .

First, we give an intuitive analysis on the construction of the proposed preconditioner. In Remark A.2 it is mentioned that the distance  $\omega$  of the two solutions  $x_c := \arg \min f_c(x)$  and  $x_{c,\mu} := \arg \min f_c^\mu(x)$  can be arbitrarily small for sufficiently small values of  $\mu$ . Moreover, according to Assumption 1.2,  $W^*x_c$  is  $q$  sparse. Therefore, Remark A.2 implies that  $W^*x_{c,\mu}$  is approximately  $q$  sparse with nearly zero components of  $\mathcal{O}(\omega)$ . A consequence of the previous statement is that the components of  $W^*x_{c,\mu}$  split into the following disjoint sets

$$\mathcal{B} := \{i \in \{1, 2, \dots, l\} \mid |W_i^*x_{c,\mu}| \gg \mathcal{O}(\omega)\}, \quad |\mathcal{B}| = q = |\text{supp}(W^*x_c)|,$$

$$\mathcal{B}^c := \{i \in \{1, 2, \dots, l\} \mid |W_i^*x_{c,\mu}| \approx \mathcal{O}(\omega)\}, \quad |\mathcal{B}^c| = l - q.$$

The behaviour of  $W^*x_{c,\mu}$  has a crucial influence on matrix  $\nabla^2 \psi_\mu(W^*x_{c,\mu})$  in (2.6). Notice that the components of the diagonal matrix  $D$ , defined in (2.5) as part of  $\nabla^2 \psi_\mu(W^*x_{c,\mu})$ , split into two disjoint sets. In particular,  $q$  components are non-zeros much less than  $\mathcal{O}(1/\omega)$ , while the majority,  $l - q$ , of its components are of  $\mathcal{O}(1/\omega)$ ,

$$(5.1) \quad D_i \ll \mathcal{O}\left(\frac{1}{\omega}\right) \quad \forall i \in \mathcal{B} \quad \text{and} \quad D_i = \mathcal{O}\left(\frac{1}{\omega}\right) \quad \forall i \in \mathcal{B}^c.$$

- 1: **Input:**  $\tau_1 \in (0, 1)$ ,  $\tau_2 \in (0, 1/2)$ ,  $x^0$ ,  $g_{re}^0$  and  $g_{im}^0$ , where  $\|g_{re}^0 + \sqrt{-1}g_{im}^0\|_\infty \leq 1$ .
- 2: **Loop:** For  $k = 1, 2, \dots$ , until termination criteria are met.
- 3: Calculate  $\Delta x^k$ ,  $\Delta g_{re}^k$  and  $\Delta g_{im}^k$  by solving approximately the system (4.4), until (4.6) is satisfied for some  $\eta \in [0, 1)$ .
- 4: Set  $\tilde{g}_{re}^{k+1} := g_{re}^k + \Delta g_{re}^k$ ,  $\tilde{g}_{im}^{k+1} := g_{im}^k + \Delta g_{im}^k$  and calculate

$$\bar{g}^{k+1} := P_{\|\cdot\|_\infty \leq 1}(\tilde{g}_{re}^{k+1} + \sqrt{-1}\tilde{g}_{im}^{k+1}),$$

where  $P_{\|\cdot\|_\infty \leq 1}(\cdot)$  is the orthogonal projection on the  $\ell_\infty$  ball.

Then set  $g_{re}^{k+1} := \text{Re}\bar{g}^{k+1}$  and  $g_{im}^{k+1} := \text{Im}\bar{g}^{k+1}$ .

- 5: Find the least integer  $j \geq 0$  such that

$$f_c^\mu(x^k + \tau_1^j \Delta x^k) \leq f_c^\mu(x^k) + \tau_2 \tau_1^j (\nabla f_c^\mu(x^k))^\top \Delta x^k$$

and set  $\alpha := \tau_1^j$ .

- 6: Set  $x^{k+1} := x^k + \alpha \Delta x^k$ .

Fig. 4.1: Algorithm primal-dual Newton Conjugate Gradients

Hence, for points close to  $x_{c,\mu}$  and small  $\mu$ , matrix  $\nabla^2 f_c^\mu(x)$  in (2.8) consists of a dominant matrix  $c\nabla^2 \psi_\mu(x)$  and of matrix  $A^\top A$  with moderate largest eigenvalue. The previous argument for  $A^\top A$  is due to (1.3). Observe that  $\lambda_{\max}(A^\top A) = \lambda_{\max}(AA^\top)$ , hence, if  $\delta$  in (1.3) is not a very large constant, then  $\lambda_{\max}(A^\top A) \leq 1 + \delta$ . According to Remark 4.2, the symmetric matrix  $\text{sym}(\tilde{B})$  in (2.8) tends to matrix  $\nabla^2 \psi_\mu(x)$  as  $x \rightarrow x_{c,\mu}$ . Therefore, matrix  $\text{sym}(\tilde{B})$  is the dominant matrix in  $\hat{B}$ . For this reason, in the proposed preconditioning technique, matrix  $A^\top A$  in (2.8) is replaced by a scaled identity  $\rho I_n$ ,  $\rho > 0$ , while the dominant matrix  $\text{sym}(\tilde{B})$  is maintained. Based on these observations we propose the following preconditioner

$$(5.2) \quad \tilde{N} := c \text{sym}(\tilde{B}) + \rho I_n.$$

In order to capture the approximate separability of the diagonal components of matrix  $D$  for points close to  $x_{c,\mu}$ , when  $\mu$  is sufficiently small, we will work with approximate guess of  $\mathcal{B}$  and  $\mathcal{B}^c$ . For this reason, we introduce the positive constant  $\nu$ , such that

$$\#(D_i < \nu) = \sigma.$$

Here  $\sigma$  might be different from the sparsity of  $W^*x_c$ . Furthermore, according to the above definition we have the sets

$$(5.3) \quad \mathcal{B}_\nu := \{i \in \{1, 2, \dots, l\} \mid D_i < \nu\} \quad \text{and} \quad \mathcal{B}_\nu^c := \{1, 2, \dots, l\} \setminus \mathcal{B}_\nu,$$

with  $|\mathcal{B}_\nu| = \sigma$  and  $|\mathcal{B}_\nu^c| = l - \sigma$ . This notation is being used in the following theorem, in which we analyze the behaviour of the spectral properties of preconditioned  $\nabla^2 f_c^\mu(x)$ , with preconditioner  $N := c\nabla^2 \psi_\mu(W^*x) + \rho I_n$ . However, according to Remark 4.2 matrices  $\hat{B}$  and  $\tilde{N}$  tend to  $\nabla^2 f_c^\mu(x)$  and  $N$ , respectively, as  $x \rightarrow x_{c,\mu}$ . Therefore, the following theorem is useful for the analysis of the limiting behaviour of the spectrum of preconditioned  $\hat{B}$ .



THEOREM 5.1. Let  $\nu$  be any positive constant and  $\#(D_i < \nu) = \sigma$  at a point  $x$ , where  $D$  is defined in (2.5). Let

$$\nabla^2 f_c^\mu(x) = c\nabla^2 \psi_\mu(W^*x) + A^\top A \quad \text{and} \quad N := c\nabla^2 \psi_\mu(W^*x) + \rho I_n.$$

Additionally, let  $A$  and  $W$  satisfy  $W$ -RIP with some constant  $\delta_\sigma < 1/2$  and let  $A$  satisfy (1.3) for some constant  $\delta \geq 0$ .

If the eigenvectors of  $N^{-\frac{1}{2}} \nabla^2 f_c^\mu(x) N^{-\frac{1}{2}}$  do not belong in  $\text{Ker}(W_{\mathcal{B}_\nu^c}^*)$  and  $\rho \in [\delta_\sigma, 1/2]$ , then the eigenvalues of  $N^{-1} \nabla^2 f_c^\mu(x)$  satisfy

$$|\lambda - 1| \leq \frac{1}{2} \frac{\chi + 1 + (5\chi^2 - 2\chi + 1)^{\frac{1}{2}}}{c\mu^2\nu^3\lambda_{\min}(\text{Re}(W_{\mathcal{B}_\nu^c}W_{\mathcal{B}_\nu^c}^*)) + \rho},$$

where  $\lambda \in \text{spec}(N^{-1} \nabla^2 f_c^\mu(x))$ ,  $\lambda_{\min}(\text{Re}(W_{\mathcal{B}_\nu^c}W_{\mathcal{B}_\nu^c}^*))$  is the minimum nonzero eigenvalue of  $\text{Re}(W_{\mathcal{B}_\nu^c}W_{\mathcal{B}_\nu^c}^*)$  and  $\chi := 1 + \delta - \rho$ .

If the eigenvectors of  $N^{-\frac{1}{2}} \nabla^2 f_c^\mu(x) N^{-\frac{1}{2}}$  belong in  $\text{Ker}(W_{\mathcal{B}_\nu^c}^*)$ , then

$$|\lambda - 1| \leq \frac{1}{2} \frac{\chi + 1 + (5\chi^2 - 2\chi + 1)^{\frac{1}{2}}}{\rho}.$$

*Proof.* We analyze the spectrum of matrix  $N^{-\frac{1}{2}} \nabla^2 f_c^\mu(x) N^{-\frac{1}{2}}$  instead, because it has the same eigenvalues as matrix  $N^{-1} \nabla^2 f_c^\mu(x)$ . We have that

$$\begin{aligned} N^{-\frac{1}{2}} \nabla^2 f_c^\mu(x) N^{-\frac{1}{2}} &= N^{-\frac{1}{2}} (c\nabla^2 \psi_\mu(x) + A^\top A) N^{-\frac{1}{2}} \\ &= N^{-\frac{1}{2}} (c\nabla^2 \psi_\mu(x) + A^\top A + \rho I_n - \rho I_n) N^{-\frac{1}{2}} \\ &= N^{-\frac{1}{2}} (c\nabla^2 \psi_\mu(x) + \rho I_n) N^{-\frac{1}{2}} + N^{-\frac{1}{2}} A^\top A N^{-\frac{1}{2}} - \rho N^{-1} \\ &= I_n + N^{-\frac{1}{2}} A^\top A N^{-\frac{1}{2}} - \rho N^{-1} \end{aligned}$$

Let  $u$  be an eigenvector of  $N^{-\frac{1}{2}} \nabla^2 f_c^\mu(x) N^{-\frac{1}{2}}$  with  $\|u\|_2 = 1$  and  $\lambda$  the corresponding eigenvalue, then

$$\begin{aligned} (I_n + N^{-\frac{1}{2}} A^\top A N^{-\frac{1}{2}} - \rho N^{-1})u &= \lambda u && \Longleftrightarrow \\ (N + N^{\frac{1}{2}} A^\top A N^{-\frac{1}{2}} - \rho I_n)u &= \lambda Nu && \Longrightarrow \\ u^\top N^{\frac{1}{2}} (A^\top A - \rho I_n) N^{-\frac{1}{2}} u &= (\lambda - 1)u^\top Nu && \Longrightarrow \\ (5.4) \quad |u^\top N^{\frac{1}{2}} (A^\top A - \rho I_n) N^{-\frac{1}{2}} u| &= |\lambda - 1|u^\top Nu. \end{aligned}$$

First, we find an upper bound for  $|u^\top N^{\frac{1}{2}} (A^\top A - \rho I_n) N^{-\frac{1}{2}} u|$ . Matrices  $N^{\frac{1}{2}} (A^\top A - \rho I_n) N^{-\frac{1}{2}}$  and  $A^\top A - \rho I_n$  have the same eigenvalues. Therefore,

$$|u^\top N^{\frac{1}{2}} (A^\top A - \rho I_n) N^{-\frac{1}{2}} u| \leq \lambda_{\max}^+(A^\top A - \rho I_n)$$

where  $\lambda_{\max}^+(\cdot)$  is the largest eigenvalue of the input matrix in absolute value. Thus,

$$\begin{aligned} |u^\top N^{\frac{1}{2}} (A^\top A - \rho I_n) N^{-\frac{1}{2}} u| &\leq \max_{\|v\|_2^2 \leq 1} |v^\top (A^\top A - \rho I_n) v| \\ &= \max_{\|Pv\|_2^2 + \|Qv\|_2^2 \leq 1} |(Pv + Qv)^\top (A^\top A - \rho I_n) (Pv + Qv)|, \end{aligned}$$

where  $P$  is the projection matrix to the column space of  $W_{\mathcal{B}_\nu}$  and  $Q = I_n - P$ . Using triangular inequality we get

$$\begin{aligned} |u^\top N^{\frac{1}{2}}(A^\top A - \rho I_n)N^{-\frac{1}{2}}u| &\leq \max_{\|Pv\|_2^2 + \|Qv\|_2^2 \leq 1} (|(Pv)^\top (A^\top A - \rho I_n)Pv| \\ &\quad + |(Qv)^\top (A^\top A - \rho I_n)Qv| + 2|(Pv)^\top (A^\top A - \rho I_n)Qv|). \end{aligned}$$

Let us denote by  $\hat{v}$  the solution of this maximization problem and set  $\|P\hat{v}\|_2^2 = \alpha$  and  $\|Q\hat{v}\|_2^2 = 1 - \alpha$ , where  $\alpha \in [0, 1]$ , then

$$(5.5) \quad \begin{aligned} |u^\top N^{\frac{1}{2}}(A^\top A - \rho I_n)N^{-\frac{1}{2}}u| &\leq (|(P\hat{v})^\top (A^\top A - \rho I_n)P\hat{v}| \\ &\quad + |(Q\hat{v})^\top (A^\top A - \rho I_n)Q\hat{v}| + 2|(P\hat{v})^\top (A^\top A - \rho I_n)Q\hat{v}|). \end{aligned}$$

Since  $P\hat{v}$  belongs to the column space of  $W_{\mathcal{B}_\nu}$  and  $|\mathcal{B}_\nu| = \sigma$ , from W-RIP with  $\delta_\sigma < 1/2$  we have that

$$\begin{aligned} \|P\hat{v}\|_2^2(1 - \delta_\sigma) &\leq \|AP\hat{v}\|_2^2 && \implies \\ \|P\hat{v}\|_2^2(1 - \rho) &\leq \|AP\hat{v}\|_2^2 && \iff \\ \|P\hat{v}\|_2^2(1 - 2\rho) &\leq \|AP\hat{v}\|_2^2 - \rho\|P\hat{v}\|_2^2. \end{aligned}$$

Since  $\rho \in [\delta_\sigma, 1/2]$  we have that  $\rho\|P\hat{v}\|_2^2 \leq \|AP\hat{v}\|_2^2$ , which implies that if the eigenvector corresponding to an eigenvalue of matrix  $A^\top A$  belongs to the column space of  $W_{\mathcal{B}_\nu}$ , then the eigenvalue cannot be smaller than  $\rho$ . Hence,

$$|(P\hat{v})^\top (A^\top A - \rho I_n)P\hat{v}| \leq |(P\hat{v})^*(A^\top A - \rho I_n)P\hat{v}| = (P\hat{v})^*(A^\top A - \rho I_n)P\hat{v}.$$

Moreover, from W-RIP with  $\delta_\sigma < 1/2$  and  $\rho \in [\delta_\sigma, 1/2]$ , we also have that  $(P\hat{v})^*(A^\top A - \rho I_n)P\hat{v} \leq \|P\hat{v}\|_2^2$ . Thus,

$$(5.6) \quad |(P\hat{v})^\top (A^\top A - \rho I_n)P\hat{v}| \leq \alpha.$$

From property (1.3) and  $\lambda_{\max}(A^\top A) = \lambda_{\max}(AA^\top)$ , we have that  $\lambda_{\max}(A^\top A - \rho I_n) \leq 1 + \delta - \rho$ . Finally, using the Cauchy-Schwarz inequality, we get that

$$(5.7) \quad |(Q\hat{v})^\top (A^\top A - \rho I_n)Q\hat{v}| \leq (1 + \delta - \rho)(1 - \alpha)$$

and

$$(5.8) \quad |(P\hat{v})^\top (A^\top A - \rho I_n)Q\hat{v}| \leq (1 + \delta - \rho)\sqrt{\alpha(1 - \alpha)}.$$

Using (5.6), (5.7) and (5.8) in (5.5) we have that

$$(5.9) \quad |u^\top N^{\frac{1}{2}}(A^\top A - \rho I_n)N^{-\frac{1}{2}}u| \leq \alpha + (1 + \delta - \rho)(1 - \alpha) + 2(1 + \delta - \rho)\sqrt{\alpha(1 - \alpha)}.$$

Set  $\chi := 1 + \delta - \rho$ , it is easy to check that in the interval  $\alpha \in [0, 1]$  the right hand side of (5.9) has a maximum at one of the four candidate points

$$\alpha_1 = 0, \quad \alpha_2 = 1, \quad \alpha_{3,4} = \frac{1}{2} \left( 1 \pm \left( \frac{(\chi - 1)^2}{5\chi^2 - 2\chi + 1} \right)^{1/2} \right),$$

where  $\alpha_3$  is for plus and  $\alpha_4$  is for minus. The corresponding function values are

$$\chi, \quad 1, \quad \frac{\chi + 1}{2} + \frac{1}{2} \frac{3\chi^2 + 2\chi - 1}{(5\chi^2 - 2\chi + 1)^{1/2}}, \quad \frac{\chi + 1}{2} + \frac{1}{2} (5\chi^2 - 2\chi + 1)^{1/2},$$

respectively. Hence, the maximum among these four values is given for  $\alpha_4$ . Thus, (5.9) is upper bounded by

$$(5.10) \quad |u^\top N^{\frac{1}{2}}(A^\top A - \rho I_n)N^{-\frac{1}{2}}u| \leq \frac{\chi + 1}{2} + \frac{1}{2}(5\chi^2 - 2\chi + 1)^{\frac{1}{2}}.$$

We now find a lower bound for  $u^\top Nu$ . Using the definition of  $D$  in (2.5), matrix  $\hat{Y}$  in (2.7) is rewritten as  $\hat{Y}_i = (2\mu^2 + |y_i|^2)D_i^3 \forall i = 1, 2, \dots, l$ . Thus  $\nabla^2 \psi_\mu(x)$  in (2.6) is rewritten as

$$(5.11) \quad \begin{aligned} \nabla^2 \psi_\mu(W^*x) &= \frac{1}{4}[(W\tilde{D}^3W^* + \bar{W}\tilde{D}^3\bar{W}^* + W\tilde{Y}\bar{W}^* + \bar{W}\tilde{Y}W^*) \\ &\quad + 2\mu^2(WD^3W^* + \bar{W}D^3\bar{W}^*)], \end{aligned}$$

where  $\tilde{D}_i = |y_i|^2 D_i^3 \forall i = 1, 2, \dots, l$ . Observe, that matrix  $\nabla^2 \psi_\mu(W^*x)$  consists of two matrices  $W\tilde{D}^3W^* + \bar{W}\tilde{D}^3\bar{W}^* + W\tilde{Y}\bar{W}^* + \bar{W}\tilde{Y}W^*$  and  $2\mu^2(WD^3W^* + \bar{W}D^3\bar{W}^*)$  which are positive semi-definite. Using (5.11) and the previous statement we get that

$$\begin{aligned} u^\top Nu &= u^\top (c\nabla^2 \psi_\mu(W^*x) + \rho I_n)u \\ &= \frac{c}{4}u^\top (W\hat{Y}W^* + \bar{W}\hat{Y}\bar{W}^* + W\tilde{Y}\bar{W}^* + \bar{W}\tilde{Y}W^*)u + \rho \\ &\geq \frac{c\mu^2}{2}u^\top (WD^3W^* + \bar{W}D^3\bar{W}^*)u + \rho. \end{aligned}$$

Furthermore, using the splitting of matrix  $D$  (5.3), the last inequality is equivalent to

$$\begin{aligned} u^\top Nu &= \frac{c\mu^2}{2}u^\top (W_{\mathcal{B}_\nu} D_{\mathcal{B}_\nu}^3 W_{\mathcal{B}_\nu}^* + W_{\mathcal{B}_\nu^c} D_{\mathcal{B}_\nu^c}^3 W_{\mathcal{B}_\nu^c}^* + \bar{W}_{\mathcal{B}_\nu} D_{\mathcal{B}_\nu}^3 \bar{W}_{\mathcal{B}_\nu}^* + \bar{W}_{\mathcal{B}_\nu^c} D_{\mathcal{B}_\nu^c}^3 \bar{W}_{\mathcal{B}_\nu^c}^*)u + \rho \\ &\geq \frac{c\mu^2}{2}u^\top (W_{\mathcal{B}_\nu^c} D_{\mathcal{B}_\nu^c}^3 W_{\mathcal{B}_\nu^c}^* + \bar{W}_{\mathcal{B}_\nu^c} D_{\mathcal{B}_\nu^c}^3 \bar{W}_{\mathcal{B}_\nu^c}^*)u + \rho. \end{aligned}$$

Using the defition of  $\mathcal{B}_\nu^c$  (5.3) in the last inequality, the quantity  $u^\top Nu$  is further lower bounded by

$$(5.12) \quad u^\top Nu \geq \frac{c\mu^2\nu^3}{2}u^\top (W_{\mathcal{B}_\nu^c} W_{\mathcal{B}_\nu^c}^* + \bar{W}_{\mathcal{B}_\nu^c} \bar{W}_{\mathcal{B}_\nu^c}^*)u + \rho.$$

If  $u \notin \text{Ker}(W_{\mathcal{B}_\nu^c}^*)$ , then from (5.12) we get

$$(5.13) \quad u^\top Nu \geq c\mu^2\nu^3\lambda_{\min}(\text{Re}(W_{\mathcal{B}_\nu^c} W_{\mathcal{B}_\nu^c}^*)) + \rho.$$

Hence, combining (5.4), (5.10) and (5.13) we conclude that

$$|\lambda - 1| \leq \frac{1}{2} \frac{\chi + 1 + (5\chi^2 - 2\chi + 1)^{\frac{1}{2}}}{c\mu^2\nu^3\lambda_{\min}(\text{Re}(W_{\mathcal{B}_\nu^c} W_{\mathcal{B}_\nu^c}^*)) + \rho}$$

If  $u \in \text{Ker}(W_{\mathcal{B}_\nu^c}^*)$ , then from (5.12) we have that  $u^\top Nu \geq \rho$ , hence

$$|\lambda - 1| \leq \frac{1}{2} \frac{\chi + 1 + (5\chi^2 - 2\chi + 1)^{\frac{1}{2}}}{\rho}.$$

□

Let us now draw some conclusions from Theorem 5.1. In order for the eigenvalues of  $N^{-1}\nabla^2 f_c^\mu(x)$  to be around one, it is required that the degree of freedom  $\nu$  is chosen such that  $\nu = \mathcal{O}(1/\mu)$  and  $\mu$  is small. For such  $\nu$ , the cardinality  $\sigma$  of the set  $\mathcal{B}_\nu$  must be small enough such that matrices  $A$  and  $W$  satisfy W-RIP with constant  $\delta_\sigma < 1/2$ ; otherwise the assumptions of Theorem 5.1 will not be satisfied. This is possible if the pdNCG iterates are close to the optimal solution  $x_{c,\mu}$  and  $\mu$  is sufficiently small. In particular, for sufficiently small  $\mu$ , from Remark A.2 we have that  $x_{c,\mu} \approx x_c$  and  $\sigma \approx q$ . According to Assumption 1.2 for the  $q$ -sparse  $x_c$ , W-RIP is satisfied for  $\delta_{2q} < 1/2 \implies \delta_q < 1/2$ . Hence, for points close to  $x_{c,\mu}$  and small  $\mu$  we expect that  $\delta_\sigma < 1/2$ . Therefore, the result in Theorem 5.1 captures only the limiting behaviour of preconditioned  $\nabla^2 f_c^\mu(x)$  as  $x \rightarrow x_{c,\mu}$ . Moreover, according to Remark 4.2, Theorem 5.1 implies that at the limit the eigenvalues of  $\tilde{N}^{-1}\hat{B}$  are also clustered around one.

The scenario of limiting behaviour of the preconditioner is pessimistic. Let  $\tilde{\sigma}$  be the minimum sparsity level such that matrices  $A$  and  $W$  are W-RIP with  $\delta_{\tilde{\sigma}} < 1/2$ . Then, according to the uniform property of W-RIP (i.e. it holds for all at most  $\tilde{\sigma}$ -sparse vectors), the preconditioner will start to be effective even if the iterates  $W^*x^k$  are approximately sparse with  $\tilde{\sigma}$  dominant non-zero components. Numerical evidence is provided in Figure 5.1 to confirm this claim.

In Figure 5.1 the spectra  $\lambda(\hat{B})$  and  $\lambda(\tilde{N}^{-1}\hat{B})$  are displayed for a sequence of systems which arise when an iTV problem is solved. For this iTV problem we set matrix  $A$  to be a partial 2D DCT,  $n = 2^{10}$ ,  $m = n/4$ ,  $c = 2.29e-2$  and  $\rho = 5.0e-1$ . For the experiment in Figures 5.1a and 5.1b the smoothing parameter has been set to  $\mu = 1.0e-3$  and in Figures 5.1c and 5.1d  $\mu = 1.0e-5$ . Observe that for both cases the eigenvalues of matrix  $\tilde{N}^{-1}\hat{B}$  are *niceily clustered around one*. On the other hand the eigenvalues of matrix  $\hat{B}$  have large variations and there are many small eigenvalues close to zero. Notice that the preconditioner was effective not only at optimality as it was predicted by theory, but through all iterations of pdNCG. This is because starting from the zero solution the iterates  $W^*x^k$  were maintained approximately sparse  $\forall k$ .

We now comment on the second result of Theorem 5.1, when the eigenvectors of  $N^{-\frac{1}{2}}\nabla^2 f_c^\mu(x)N^{-\frac{1}{2}}$  belong in  $\text{Ker}(W_{\mathcal{B}_\nu}^*)$ . In this case, according to Theorem 5.1 the preconditioner removes the disadvantageous dependence of the spectrum of  $\nabla^2 f_c^\mu(x)$  on the smoothing parameter  $\mu$ . However, there is no guarantee that the eigenvalues of  $N^{-1}\nabla^2 f_c^\mu(x)$  are clustered around one, regardless of the distance from the optimal solution  $x_{c,\mu}$ . Again, because of Remark 4.2 we expect that the spectrum of  $\tilde{N}^{-1}\hat{B}$  at the limit will have a similar behaviour.

**6. Continuation.** In the previous section we have shown that by using preconditioning, the spectral properties of systems which arise can be improved. However, for initial stages of pdNCG a similar result can be achieved without the cost of having to apply preconditioning. In particular, at initial stages the spectrum of  $\hat{B}$  can be controlled to some extent through inexpensive continuation. Whilst preconditioning is enabled only at later stages of the process. Briefly by continuation it is meant that a sequence of “easier” subproblems is solved, instead of solving directly problem (2.2). The reader is referred to Chapter 11 in [23] for a survey on continuation methods in optimization.

In this paper we use a similar continuation framework to [4, 8, 9, 14, 15]. In particular, a sequence of sub-problems (2.2) is solved, where each of them is parameterized by  $c$  and  $\mu$  simultaneously. Let  $\tilde{c}$  and  $\tilde{\mu}$  be the final parameters for which problem (2.2) must be solved. Then the number of continuation iterations  $\vartheta$  is set to be the maximum order of magnitude between  $1/\tilde{c}$  and  $1/\tilde{\mu}$ . For instance, if  $\tilde{c} = 1.0e-2$  and

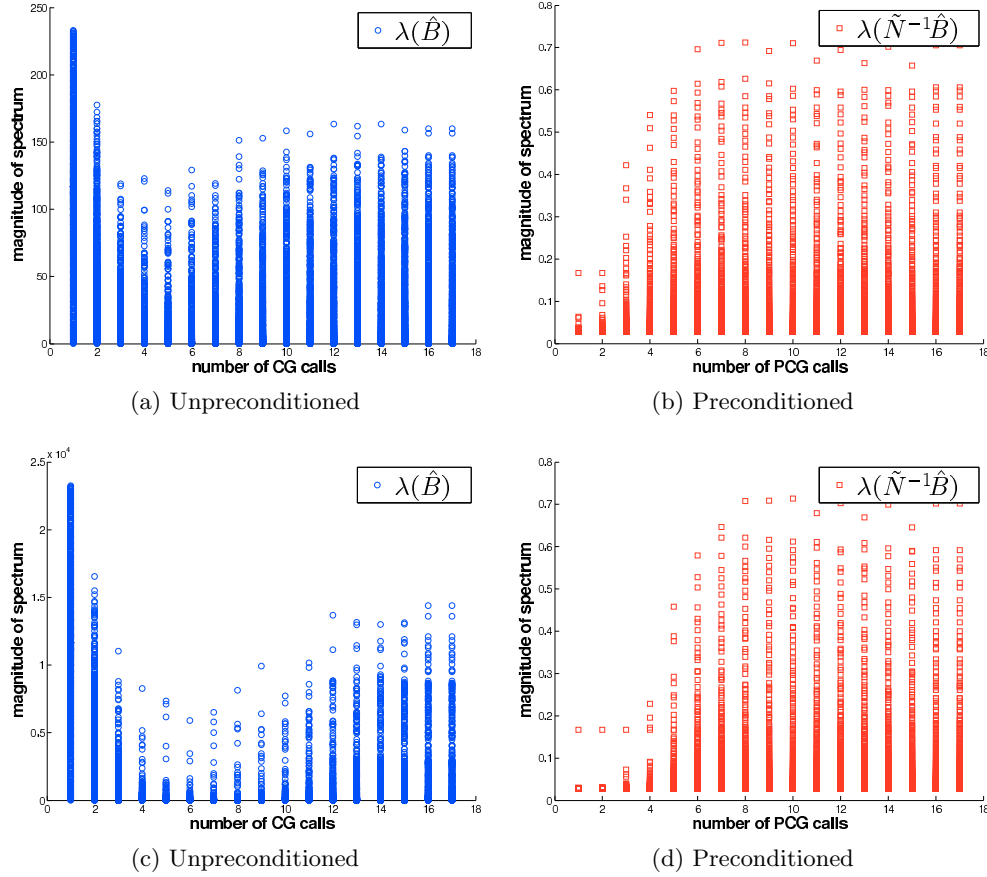


Fig. 5.1: Spectra of  $\lambda(\hat{B})$  and  $\lambda(\tilde{N}^{-1}\hat{B})$  when pdNCG is applied with smoothing parameter  $\mu = 1.0e-3$  (top sub-figures) and  $\mu = 1.0e-5$  (bottom sub-figures). Matrix  $A$  in  $\hat{B}$  is a 2D DCT,  $n = 2^{10}$ ,  $m = n/4$  and  $c = 2.29e-2$ . Seventeen systems are solved in total for each experiment.

$\tilde{\mu} = 1.0e-5$  then  $\vartheta := \max(2, 5) = 5$ . If  $\vartheta \geq 2$ , then the initial parameters  $c^0$  and  $\mu^0$  are both always set to  $1.0e-1$  and the intervals  $[c^0, \tilde{c}]$  and  $[\mu^0, \tilde{\mu}]$  are divided in  $\vartheta$  equal subintervals in logarithmic scale. For all experiments that we have reported in this paper we have found that this setting leads to a generally acceptable improvement over pdNCG without continuation. The pseudo-code of the proposed continuation framework is shown in Figure 6.1.

Figure 6.2 shows the performance of pdNCG for three cases, no continuation with preconditioning, continuation with preconditioning through the whole process and continuation with preconditioning only at later stages. The vertical axis of Figure 6.2 shows the relative error  $\|x^k - x_{\tilde{c}, \tilde{\mu}}\|_2 / \|x_{\tilde{c}, \tilde{\mu}}\|_2$ . The optimal  $x_{\tilde{c}, \tilde{\mu}}$  is obtained by using pdNCG with parameter tuning set to recover a highly accurate solution. The horizontal axis shows the CPU time. The problem is an iTV problem where matrix  $A$  is a partial 2D DCT,  $n = 2^{16}$ ,  $m = n/4$ ,  $c = 5.39e-2$  and  $\rho = 5.0e-1$ . The final smoothing parameter  $\tilde{\mu}$  is set to  $1.0e-5$ . For the experiment that preconditioning is

- 1: **Outer loop:** For  $j = 0, 1, 2, \dots, \vartheta$ , produce  $(c^j, \mu^j)_{j=0}^\vartheta$ .
- 2: **Inner loop:** Approximately solve the subproblem

$$\text{minimize } f_{c^j}^{\mu^j}(x)$$

using pdNCG and by initializing it with the solution of the previous subproblem.

Fig. 6.1: Continuation framework

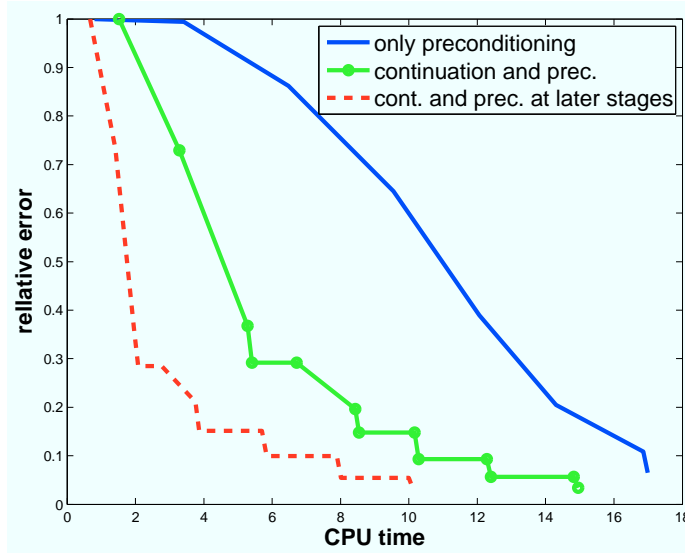


Fig. 6.2: Performance of pdNCG for three different settings, i) no continuation with preconditioning, ii) continuation with preconditioning through all iterations and iii) continuation with preconditioning only at later stages. The vertical axis presents the relative error  $\|x^k - x_{\tilde{c}, \tilde{\mu}}\|_2 / \|x_{\tilde{c}, \tilde{\mu}}\|_2$ , where  $x_{\tilde{c}, \tilde{\mu}}$  is the optimal solution for the parameter setting  $\tilde{c}, \tilde{\mu}$  in problem (2.2).

used only at later stages of continuation; preconditioning is enabled when  $\mu^j \leq 1.0e-4$ , where  $j$  is the counter for continuation iterations. All experiments are terminated when the relative error  $\|x^k - x_{\tilde{c}, \tilde{\mu}}\|_2 / \|x_{\tilde{c}, \tilde{\mu}}\|_2 \leq 1.0e-1$ . Solving approximately the problem is an acceptable practise since the problem is very noisy (i.e. signal-to-noise-ratio is 10 decibel) and there is not much improvement of the reconstructed image if more accurate solutions are requested. Finally, all other parameters of pdNCG were set to the same values for all three experiments. Observe in Figure 6.2 that continuation with preconditioning only at late stages was the best approach for this problem.

**7. Numerical experiments.** In this section we demonstrate the efficiency of pdNCG against state-of-the-art methods for  $\ell_1$ -analysis problems with coherent and redundant dictionaries. In what follows we briefly discuss existing methods, we describe the setting of the experiments and finally numerical results are presented. All

experiments that are demonstrated in this paper can be reproduced by downloading the software from <http://www.maths.ed.ac.uk/ERGO/pdNCG/>.

**7.1. Existing algorithms.** We compare pdNCG with two state-of-the-art first-order methods, TFOCS [5] and TVAL3 [17].

- TFOCS (Templates for First-Order Conic Solvers) is a MATLAB software for the solution of signal reconstruction problems. TFOCS solves the dual problem of

$$(7.1) \quad \text{minimize } c\|W^*x\|_1 + \frac{\mu_{T_1}}{2}\|x - x^0\|_2^2 + \frac{1}{2}\|Ax - b\|_2^2,$$

where  $\mu_{T_1}$  is a positive constant. TFOCS also solves the dual problem of

$$(7.2) \quad \begin{aligned} \min_{x \in \mathbb{R}^n} \quad & \|W^*x\|_1 + \frac{\mu_{T_2}}{2}\|x - x^0\|_2^2 \\ \text{subject to: } \quad & \|Ax - b\|_2 \leq \epsilon, \end{aligned}$$

where  $\epsilon > 0$ . Although problems (7.1) and (7.2) are non-smooth, the regularization terms  $\mu_{T_1}/2\|x - x^0\|_2^2$  and  $\mu_{T_2}/2\|x - x^0\|_2^2$  yield smooth convex dual problems, which can be solved by standard first-order methods. In particular, the smooth dual problems are solved using the Auslender and Teboulle's accelerated first-order method [2]. In our experiments we present results for TFOCS for both problems (7.1) and (7.2). We denote by TFOCS\_unc the version that solves the unconstrained problem (7.1) and by TFOCS\_con the version that solves the constrained problem (7.2). TFOCS can be downloaded from [5].

- TVAL3 (Total-Variation minimization by Augmented Lagrangian and ALternating direction ALgorithms) is a MATLAB software for the solution of signal reconstruction problems regularized with the total-variation semi-norm. TVAL3 reformulates problem (1.1) to the equivalent problem

$$(7.3) \quad \text{minimize } \sum_{i=1}^l \|\Omega_i^\top x\|_2 + \frac{1}{2}\|Ax - b\|_2^2,$$

where  $\Omega_i = [ReW_i, ImW_i] \in \mathbb{R}^{n \times 2}$ . Then it solves the augmented Lagrangian reformulation of problem (7.3), which is

$$(7.4) \quad \text{minimize } \sum_{i=1}^l (\|u_i\|_2 + \frac{\beta}{2}\|\Omega_i^\top x - u_i\|_2^2 - v_i^\top(\Omega_i^\top x - u_i)) + \frac{1}{2}\|Ax - b\|_2^2,$$

where  $u_i, v_i \in \mathbb{R}^2$  and  $\beta$  is a positive constant. The augmented Lagrangian in (7.4) is minimized for variables  $x \in \mathbb{R}^n$  and  $u_i$   $i = 1, 2, \dots, l$ . The parameters  $v_i$   $i = 1, 2, \dots, l$  are handled by the method.

Other solvers are NestA [4] and C-SALSA [1], which can also solve (1.1) but they are applicable only in the case that  $(AA^\top)^{-1}$  is available. Another method is the Primal-Dual Hybrid Gradient (PDHG) in [12]. PDHG has been reported to be very efficient for imaging applications such as denoising and deblurring, for which matrix  $A$  is the identity or a square and full-rank matrix which is inexpensively diagonalizable. Unfortunately, this is not the case for the CS problems that we are interested in. However, for all previous methods the matrix inversion can be replaced with a solution of a linear system at every iteration of the methods or a one-time cost of

a factorization. To the best of our knowledge, there are no available implementations with such modifications for these methods.

There exists also a generic proximal algorithm for total-variation [10] and the Generalized Iterative Soft Thresholding (GISTA) in [18] for which we do not have generic implementations for CS problems.

**7.2. Equivalent problems.** Solvers pdNCG, TFOCS and TVAL3 solve similar but not equivalent problems. In particular, pdNCG solves problem (2.2), which is parameterized by  $c$  and  $\mu$ . TFOCS solves problems (7.1) and (7.2), which are parameterized by  $c$ ,  $\mu_{T_1}$  and  $\mu_{T_2}$ ,  $\epsilon$ , respectively. TVAL3 solves problem (7.4), which is parameterized by  $c$  and  $\beta$ .

In our experiments we put significant effort in calibrating parameters  $c$ ,  $\mu$ ,  $\mu_{T_1}$ ,  $\mu_{T_2}$ ,  $\epsilon$  and  $\beta$  such that all methods solve similar problems. First, we set  $\epsilon = \|b - \tilde{b}\|_2$  in (7.2), where  $\tilde{b}$  is the noiseless sampled signal. Hence problem (7.2) is parameterized with the optimal  $\epsilon$ . Then we find an approximation of the optimal  $c$ . By optimal  $c$  we mean the value of  $c$  for which problems (1.1) and (7.2) are equivalent if  $\epsilon = \|b - \tilde{b}\|_2$  and  $\mu_{T_2} = 0$ . Let  $\omega$  denote the optimal Lagrange multiplier of (7.2). If  $\epsilon = \|b - \tilde{b}\|_2$  and  $\mu_{T_2} = 0$ , then it is easy to show that for  $c := 2/\omega$  problems (1.1) and (7.2) are equivalent.

The exact optimal Lagrange multiplier  $\omega$  is not known a-priori. However it can be calculated by solving to high accuracy the dual problem of (7.1) with TFOCS. Unfortunately, the majority of the experiments that we perform are large scale and TFOCS converges slowly for  $\mu_{T_2} \approx 0$ . For this reason, we first solve (7.2) using TFOCS with a moderate  $\mu_{T_2}$ , in order to obtain an approximate optimal Lagrange multiplier  $\omega$  in reasonable CPU time. Then we set  $c := 2\gamma/\omega$ , where  $\gamma$  is a small positive constant, which is calculated experimentally such that problems (1.1) and (7.2) have similar solution. If  $\tilde{b}$  is not available, then  $\epsilon$  is set such that a visually pleasant solution is obtained.

The smoothing parameters  $\mu_{T_1}$  and  $\mu_{T_2}$  of TFOCS in (7.1) and (7.2), respectively, are set such that the corresponding obtained solutions have small relative error. Let  $x_{T_1}$  and  $x_{T_2}$  denote the obtained solutions from problems (7.1) and (7.2), then  $\|x_{T_2} - \tilde{x}\|_2/\|\tilde{x}\|_2$  and  $\|x_{T_2} - \tilde{x}\|_2/\|\tilde{x}\|_2$  are of  $\mathcal{O}(10^{-1})$  or  $\mathcal{O}(10^{-2})$ , where  $\tilde{x}$  is the known optimal noiseless solution. If  $\tilde{x}$  is not available,  $\mu_{T_1}$  and  $\mu_{T_2}$  are set such that visually pleasant reconstructions are obtained.

The smoothing parameter  $\mu$  of pdNCG is set such that  $\|x_{pd} - \tilde{x}\|_2/\|\tilde{x}\|_2$  is also  $\mathcal{O}(10^{-1})$  or  $\mathcal{O}(10^{-2})$ , where  $x_{pd}$  is the approximate optimal solution obtained by pdNCG. For all experiments that were performed the relative error between the solution of TFOCS and pdNCG is of  $\mathcal{O}(10^{-2})$ .

For TVAL3 parameter  $\beta$  is set experimentally such that  $\|x_{tv} - \tilde{x}\|_2/\|\tilde{x}\|_2$  is  $\mathcal{O}(10^{-1})$  or  $\mathcal{O}(10^{-2})$ , where  $x_{tv}$  is the approximate optimal solution obtained by TVAL3. Also, in all experiments TVAL3 obtained similar solution to TFOCS and pdNCG. For TVAL3 we have taken into account the comments of its authors that TVAL3 performs better for  $\beta \in [2^4, 2^{13}]$ . However, occasionally we had to set  $\beta = 2^2$  in order to obtain a solution which was as visually pleasing as the solutions obtained from TFOCS and pdNCG.

**7.3. Termination criteria, parameter tuning and hardware.** The version 1.3.1 of TFOCS has been used. The termination criterion of TFOCS is by default the relative step-length. The tolerance for this criterion is set to the default value, except in cases that certain suggestions are made in TFOCS software package or the corresponding paper [5]. The default Auslender and Teboulle's single-projection



method is used as a solver for TFOCS. Moreover, as suggested by the authors of TFOCS, appropriate scaling is performed on matrices  $A$  and  $W$ , such that they have approximately the same Euclidean norms. All other parameters are set to their default values, except in cases that specific suggestions are made by the authors. Generally, regarding tuning of TFOCS, substantial effort has been made in guaranteeing that problems are not over-solved.

Regarding pdNCG, parameter  $\eta$  in (4.6) is set to  $1.0e-1$ , the maximum number of backtracking line-search iterations is fixed to 10. Moreover, the backtracking line-search parameters  $\tau_1$  and  $\tau_2$  in step 4 of pdNCG (Fig. 4.1) are set to  $9.0e-1$  and  $1.0e-3$ , respectively. For iTV the preconditioner is a five-diagonal matrix, hence systems with it are solved exactly. Finally, the constant  $\rho$  of the preconditioner in (5.2) is set to  $5.0e-1$ .

Regarding TVAL3, we fix the number of maximum iterations to 1000 and any other parameters that were not discussed previously are set to their default values.

All solvers are MATLAB implementations and all experiments are run on a MacBook Air running OS X 10.10.1 with 2 GHz (3 GHz turbo boost) Intel Core Duo i7 processor using MATLAB R2012a. The cores were working with frequency 2.7 - 3 GHz during the experiments and we did not observe any CPU throttling.

**7.4. Problems sets.** We compare the solvers pdNCG, TFOCS and TVAL3 on image reconstruction problems which are modelled using iTV. We separate the images to be reconstructed into two sets, which are shown in Figures 7.1 and 7.2.

Figure 7.1 includes some standard images from the image processing community. There are seven images in total, the house and the peppers, which have  $256 \times 256$  pixels and Lena, the fingerprint, the boat and Barbara, which have  $512 \times 512$  pixels. Finally, the image Shepp-Logan has variable size depending on the experiment.

Figure 7.2 includes images which have been sampled using a single-pixel camera [11]. Briefly a single-pixel camera samples random linear projections of pixels of an image, instead of directly sampling pixels. The problem set can be downloaded from <http://dsp.rice.edu/cscamera>. In this set there are in total five sampled images, the dice, the ball, the mug the letter R and the logo. Each image has  $64 \times 64$  pixels.

**7.5. Dependence of pdNCG on smoothing parameter.** In this subsection we present the performance of pdNCG for decreasing values of the smoothing parameter  $\mu$ . For this experiments we use the images from Figures 7.1a to 7.1f. The CS matrix for all experiments is a partial Discrete Cosine Transform (DCT) matrix with  $m \approx n/4$  and  $n$  is equal to the number of pixels of each image in Figure 7.1. For all experiments the sampled signals have Signal-to-Noise-Ratio (SNR) equal to 15 decibels (dB).

The result of the experiments are shown in Table 7.1. In Table 7.1 notice that there is always a large increase in CPU time from  $\mu = 1.0e-02$  to  $1.0e-04$ . This is because for  $\mu = 1.0e-02$  pdNCG relies only on continuation, while for values of  $\mu$  equal or smaller than  $1.0e-04$  preconditioning is necessary and it is automatically activated using the technique described in Section 6. Overall pdNCG had a stable performance with respect to the smoothing parameter  $\mu$ . We believe that the good performance of the proposed preconditioner is responsible for this result. Without the preconditioner the performance of pdNCG for  $\mu \leq 1.0e-04$  worsens noticeably; occasionally the method (without preconditioning) might stagnate.

**7.6. Dependence on problem size.** We now present the performance of methods pdNCG, TFOCS and TVAL3 as the size of the problem  $n$  increases. The image



Fig. 7.1: Benchmark images, the number of pixels for each image is given in the sub-captions . For Figure 7.1g the size varies depending on the experiment

Table 7.1: Performance of pdNCG for decreasing values of the smoothing parameter  $\mu$ . For this experiment the images from Figures 7.1a to 7.1f have been used. The table shows the CPU time in seconds required for each combination of  $\mu$  and problem

$\mu$	House	Peppers	Lena	Fingerprint	Boat	Barbara
$1.0e-02$	4	4	20	20	19	19
$1.0e-04$	9	9	43	183	43	43
$1.0e-07$	11	11	49	282	68	102
$1.0e-10$	12	13	66	282	81	103
$1.0e-13$	12	13	66	310	71	100

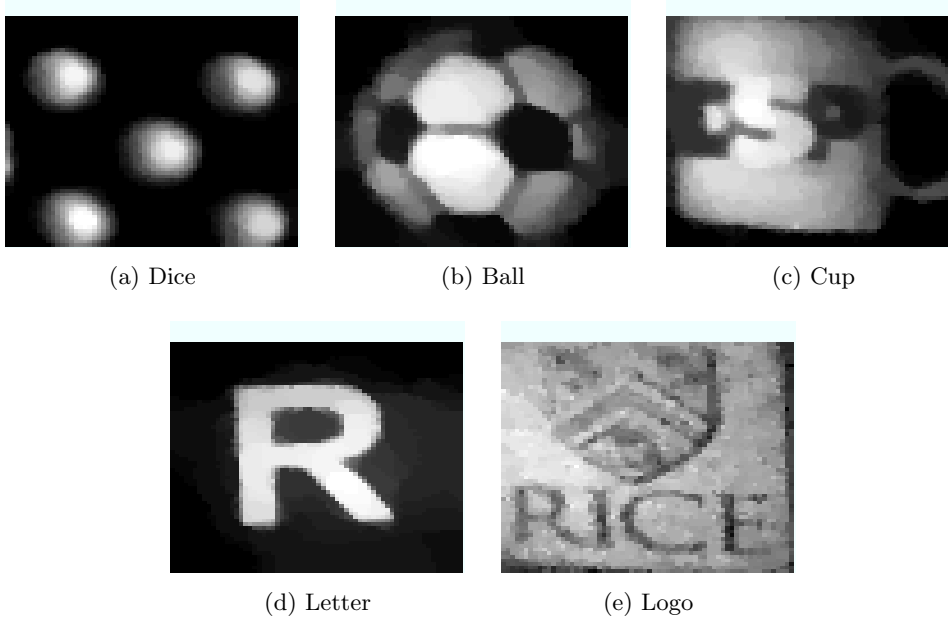


Fig. 7.2: Benchmark images, which were sampled using the single-pixel camera [11]

Table 7.2: Performance of pdNCG, TFOCS and TVAL3 for increasing problem size. The image Shepp-Logan from Figure 7.1g has been used for this experiment. The table shows the required CPU time for each solver

Solver	$64 \times 64$	$128 \times 128$	$256 \times 256$	$512 \times 512$	$1024 \times 1024$
TFOCS_con	17	23	56	260	1018
TFOCS_unc	19	30	77	378	1468
TVAL3	5	8	37	99	365
pdNCG	<b>2</b>	<b>6</b>	<b>12</b>	<b>62</b>	<b>250</b>

from Figure 7.1g has been used for this experiment. Again, the CS matrix for all experiments is a partial Discrete Cosine Transform (DCT) matrix with  $m \approx n/4$ . The sampled signals have SNR equal to 15 dB.

The results are shown in Table 7.2. Observe that all methods exhibit a linear-like increase in CPU time as a function of the size of the problem. We denote with bold the problem for which pdNCG was the fastest method.

**7.7. Dependence on the level of noise.** In this experiment we compare the solvers pdNCG, TFOCS and TVAL3 as the level of noise increases. For this experiment we use the images from Figures 7.1a to 7.1f. The CS matrix for all experiments is a partial Discrete Cosine Transform (DCT) matrix with  $m \approx n/4$ .

In Table 7.3 we present the results of this experiment. In the second column of Table 7.3 the SNR is shown, which is decreasing from 90 dB to 15 dB in six steps. The rest of the table shows the CPU time, which was required for each solver. Overall

Table 7.3: Performance of pdNCG, TFOCS and TVAL3 for increasing level of noise (decreasing SNR). SNR is measured in dB. For this experiment the images from Figures 7.1a to 7.1f have been used. The table shows the CPU time in seconds required by each solver

Solver	SNR	House	Peppers	Lena	Fingerprint	Boat	Barbara
TFOCS_con	90	57	56	261	271	264	262
	75	56	57	261	267	261	260
	60	56	56	262	274	261	260
	45	56	56	262	268	260	261
	30	56	56	260	267	260	259
	15	56	56	266	280	260	259
TFOCS_unc	90	78	78	383	397	383	378
	75	78	78	381	386	379	376
	60	78	78	381	399	380	380
	45	78	78	381	390	378	379
	30	78	78	380	382	380	379
	15	78	77	384	397	377	378
TVAL3	90	7	4	19	22	20	20
	75	7	4	18	22	19	21
	60	7	4	17	22	17	18
	45	6	4	17	23	17	19
	30	4	9	39	65	41	46
	15	13	16	60	76	61	63
pdNCG	90	18	23	114	119	122	113
	75	18	24	114	117	122	112
	60	18	24	115	114	121	113
	45	18	24	115	113	121	112
	30	19	17	78	113	78	107
	15	<b>10</b>	<b>9</b>	<b>41</b>	229	<b>44</b>	111

pdNCG has good performance for problems with large level of noise, i.e., SNR equal to 15 dB. We denote with bold the problems for which pdNCG was the fastest solver.

**7.8. Dependence on number of measurements.** In this experiment we compare the three methods for decreasing number of measurements  $m$ . For this experiment we use the images from Figures 7.1a to 7.1f. The CS matrix is a partial Discrete Cosine Transform (DCT) matrix. For all experiments the sampled signals have SNR equal to 15 dB.

The results of this experiment are shown in Table 7.4. We denote with bold the problems for which pdNCG was the fastest method.

**7.9. Single-pixel camera.** We now compare TFOCS with pdNCG on realistic image reconstruction problems where the data have been sampled using a single-pixel camera [11]. In this experiment we compare only with TFOCS\_con. This is because in all previous experiments TFOCS\_con was faster than TFOCS\_unc. Additionally, we were not able to make TVAL3 to converge to a solution which was as visually pleasant as the solutions obtained by TFOCS\_con and pdNCG. We believe that this due to the

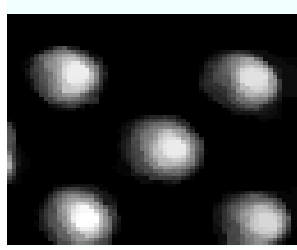
Table 7.4: Performance of pdNCG, TFOCS and TVAL3 for decreasing number of measurements  $m$ . In the second column the percentage of measurements is shown, for example 75% means that  $m \approx 3n/4$ , where  $n$  is the number of pixels in the image to be reconstructed. For this experiment the images from Figures 7.1a to 7.1f have been used. The table shows the CPU time in seconds required by each solver

Solver	m	House	Peppers	Lena	Fingerprint	Boat	Barbara
TFOCS_con	75%	61	61	255	262	260	273
	50%	60	57	260	256	263	268
	25%	57	60	253	250	273	262
TFOCS_unc	75%	80	78	367	374	375	393
	50%	85	81	374	371	383	384
	25%	77	80	370	364	380	384
TVAL3	75%	13	14	55	56	54	56
	50%	11	14	55	71	57	57
	25%	14	17	57	72	61	64
pdNCG	75%	<b>9</b>	<b>9</b>	74	196	62	108
	50%	<b>8</b>	<b>9</b>	57	217	91	106
	25%	<b>10</b>	<b>9</b>	<b>40</b>	222	<b>42</b>	113

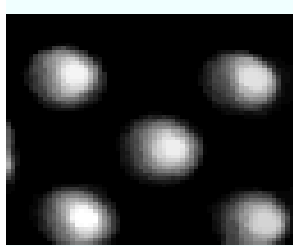
different CS matrix  $A$  in these experiments. In particular, matrix  $A \in \mathbb{R}^{m \times n}$ , where  $n = 64^2$  and  $m \approx 0.4n$ , is a partial Walsh basis which takes values 0/1 instead of  $\pm 1$ . We noticed that this matrix  $A$  does not satisfy the RIP property in Definition 1.1 with small  $\delta_q$ . Therefore, the least squares term in problem (1.1) might be ill-conditioned and this causes difficulties for TVAL3.

Moreover the optimal solutions are unknown, additionally the level of noise is unknown. Hence the reconstructed images can only be compared by visual inspection. For all four experiments 40% of measurements are selected uniformly at random.

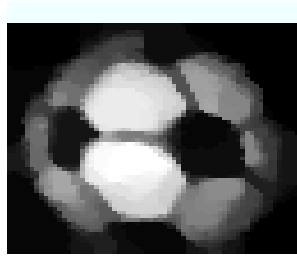
The reconstructed images by the solvers TFOCS\_con and pdNCG are presented in Figure 7.3. Solver pdNCG was faster on four out of five problems. On problems that pdNCG was faster it required on average 1.5 times less CPU time. Although it would be possible to tune pdNCG such that it is faster on all problems, we preferred to use its (simple) default tuning in order to avoid a biased comparison.



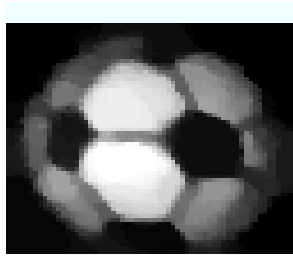
(a) TFOCS\_con, 25 sec.



(b) pdNCG, 7 sec.



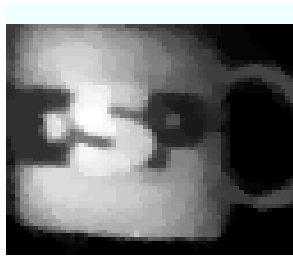
(c) TFOCS\_con, 24 sec.



(d) pdNCG, 15 sec.



(e) TFOCS\_con, 37 sec.



(f) pdNCG, 15 sec.



(g) TFOCS\_con, 26 sec.



(h) pdNCG, 27 sec.



(i) TFOCS, 49 sec.



(j) pdNCG, 33 sec.

Fig. 7.3: Experiment on realistic image reconstruction where the samples are acquired using a single-pixel camera. The subcaptions of the figures show the required seconds of CPU time for the image to be reconstructed for each solver.

**8. Conclusions.** Recently there has been great interest in the development of optimization methods for the solution of compressed sensing problems with coherent and redundant dictionaries. The methods that have been developed so far are mainly first-order methods. This is because first-order methods have inexpensive iterations and frequently offer fast initial progress in the optimization process. On the contrary, second-order methods are considered to be rather expensive. The reason is that often access to second-order information requires the solution of linear systems. In this paper we develop a second-order method, a primal-dual Newton Preconditioned Conjugate Gradients. We show that an *approximate* solution of linear systems which arise is sufficient to speed up an iterative method and additionally make it more robust. Moreover, we show that for compressed sensing problems an inexpensive preconditioner can be designed that speeds up even further the approximate solution of linear systems. Extensive numerical experiments are presented which verify our arguments. Spectral analysis of the preconditioner is performed and shows its very good limiting behaviour.

#### REFERENCES

- [1] M. V. Afonso, J. M. Bioucas-Dias, and M. A. T. Figueiredo. An augmented Lagrangian approach to the constrained optimization formulation of image inverse problems. *IEEE Transactions on Image Processing*, 20(3):681–695, 2011.
- [2] A. Auslender and Teboulle. Interior gradient and proximal methods for convex and conic optimization. *SIAM Journal on Optimization*, 16(3):697–725, 2006.
- [3] A. Beck and M. Teboulle. Smoothing and first order methods: A unified framework. *SIAM J. Optim.*, 22(2):557–580, 2012.
- [4] S. R. Becker, J. Bobin, and E. J. Candès. NestA: A fast and accurate first-order method for sparse recovery. *SIAM J. Imaging Sciences*, 4(1):1–39, 2011.
- [5] S. R. Becker, E. J. Candès, and M. C. Grant. Templates for convex cone problems with applications to sparse signal recovery. *Mathematical Programming Computation*, 3(3):165–218, 2011. <http://cvxr.com/tfocs/>.
- [6] E. J. Candès and D. L. Donoho. New tight frames of curvelets and optimal representations of objects with piecewise  $c^2$  singularities. *Comm. Pure Appl. Math.*, 57:219–266, 2004.
- [7] E. J. Candès, Y. C. Eldar, and D. Needell. Compressed sensing with coherent and redundant dictionaries. *Applied and Computational Harmonic Analysis*, 31(1):59–73, 2011.
- [8] R. H. Chan, T. F. Chan, and H. M. Zhou. Advanced signal processing algorithms. in *Proceedings of the International Society of Photo-Optical Instrumentation Engineers*, F. T. Luk, ed., SPIE, pages 314–325, 1995.
- [9] T. F. Chan, G. H. Golub, and P. Mulet. A nonlinear primal-dual method for total variation-based image restoration. *SIAM J. Sci. Comput.*, 20(6):1964–1977, 1999.
- [10] L. Condat. A generic proximal algorithm for convex optimization - Application to total-variation. *IEEE Signal Processing Letters*, 21(8):985–989, 2014.
- [11] M. F. Duarte, M. A. Davenport, D. Takhar, J. N. Laska, S. Ting, K. F. Kelly, and R. G. Baraniuk. Single-pixel imaging via compressive sampling. *IEEE Signal Processing Magazine*, 25(2):83–91, 2008. <http://dsp.rice.edu/cscamera>.
- [12] J. E. Esser. *Primal Dual Algorithms for Convex Models and Applications to Image Restoration, Registration and Nonlocal Inpainting*. PhD thesis, University of California, 2010.
- [13] K. Fountoulakis and J. Gondzio. A second-order method for strongly convex  $\ell_1$ -regularization problems. *Technical Report ERGO 14-005*, 2014.
- [14] E. T. Hale, W. Yin, and Y. Zhang. Fixed-point continuation for  $\ell_1$ -minimization: Methodology and convergence. *SIAM J. Optim.*, 19(3):1107–1130, 2008.
- [15] E. T. Hale, W. Yin, and Y. Zhang. Fixed-point continuation for  $\ell_1$ -minimization: methodology and convergence. *SIAM J. Optim.*, 19:1107–1130, 2008.
- [16] R. I. Hartley and A. Zisserman. *Multiple View Geometry in Computer Vision*. Cambridge University Press, ISBN: 0521540518, second edition, 2004.
- [17] C. Li, W. Yin, H. Jiang, and Y. Zhang. An efficient augmented Lagrangian method with applications to total variation minimization. *Computational Optimization and Applications*, 56(3):507–530, 2013.

- [18] I. Loris and C. Verhoeven. On a generalization of the iterative soft-thresholding algorithm for the case of non-separable penalty. *Inverse Problems*, 27(12):1–15, 2011.
- [19] S. Mallat. A wavelet tour of signal processing, second ed. *Academic Press, London*, 1999.
- [20] J. J. Moreau. Proximité et dualité dans un espace Hilbertien. *Bull. Soc. Math. France*, 93:273–299, 1965.
- [21] D. Needell and R. Ward. Stable image reconstruction using total variation minimization. *SIAM J. Imaging Sciences*, 6(2):1035–1058, 2013.
- [22] Y. Nesterov. Smooth minimization of non-smooth functions. *Math. Program.*, 103(1):127–152, 2004.
- [23] J. Nocedal and S. J. Wright. *Numerical Optimization*. Springer, New York, 2006.
- [24] S. Vaiter, G. Peyré, C. Dossal, and J. Fadili. Robust sparse analysis regularization. *IEEE Trans. Inf. Theory*, 59(4):2001–2016, 2013.

**Appendix A. Continuous path.** In the following lemma we show that  $x_{c,\mu} := \arg \min f_c^\mu(x)$  ( $f_c^\mu$  is defined in (2.2)) for  $c$  constant is a continuous and differentiable function of  $\mu$ .

LEMMA A.1. *Let  $c$  be constant and consider  $x_{c,\mu}$  as a functional of  $\mu$ . If condition (1.4) is satisfied, then  $x_{c,\mu}$  is continuous and differentiable.*

*Proof.* The optimality conditions of problem (2.2) are

$$c\nabla\psi_\mu(W^*x) + A^\top(Ax - b) = 0.$$

According to definition of  $x_{c,\mu}$ , we have

$$\begin{aligned} c\nabla\psi_\mu(W^*x_{c,\mu}) + A^\top(Ax_{c,\mu} - b) &= 0 & \implies \\ c\frac{d\nabla\psi_\mu(W^*x_{c,\mu})}{d\mu} + A^\top A\frac{dx_{c,\mu}}{d\mu} &= 0 & \implies \\ c\left(\nabla^2\psi_\mu(W^*x_{c,\mu})\frac{dx_{c,\mu}}{d\mu} + \frac{d\nabla\psi_\mu(W^*x)}{d\mu}\Big|_{x_{c,\mu}}\right) + A^\top A\frac{dx_{c,\mu}}{d\mu} &= 0 & \iff \\ \left(c\nabla^2\psi_\mu(W^*x_{c,\mu}) + A^\top A\right)\frac{dx_{c,\mu}}{d\mu} + c\frac{d\nabla\psi_\mu(W^*x)}{d\mu}\Big|_{x_{c,\mu}} &= 0 & \iff \\ \nabla^2 f_c^\mu(W^*x_{c,\mu})\frac{dx_{c,\mu}}{d\mu} + c\frac{d\nabla\psi_\mu(W^*x)}{d\mu}\Big|_{x_{c,\mu}} &= 0, \end{aligned}$$

where  $d\nabla\psi_\mu(W^*x)/d\mu|_{x_{c,\mu}}$  is the first-order derivative of  $\nabla\psi_\mu(W^*x)$  as a functional of  $\mu$ , measured at  $x_{c,\mu}$ . Notice that due to condition  $\text{Ker}(W^*) \cap \text{Ker}(A) = \{0\}$  we have that  $\nabla^2 f_c^\mu(x)$  is positive definite  $\forall x$ , hence  $x_{c,\mu}$  is unique. Therefore, the previous system has a unique solution, which means that  $x_{c,\mu}$  is uniquely differentiable as a functional of  $\mu$  with  $c$  being constant. Therefore,  $x_{c,\mu}$  is continuous as a functional of  $\mu$ .  $\square$

REMARK A.2. *Lemma A.1 and continuity imply that there exists sufficiently small smoothing parameter  $\mu$  such that  $\|x_{c,\mu} - x_c\|_2 < \omega$  for any arbitrarily small  $\omega > 0$ .*